Ultracompact resonator with high quality-factor based on a hybrid grating structure

Taghizadeh, Alireza; Mørk, Jesper; Chung, Il-Sug

Published in:
Optics Express

Link to article, DOI:
10.1364/OE.23.014913

Publication date:
2015

Document Version
Publisher's PDF, also known as Version of record

Ultracompact resonator with high quality-factor based on a hybrid grating structure

Alireza Taghizadeh, Jesper Mørk, and Il-Sug Chung*

Department of Photonics Engineering (DTU Fotonik), Technical University of Denmark, DK-2800 Kgs. Lyngby, Denmark

*ilch@fotonik.dtu.dk

Abstract: We numerically investigate the properties of a hybrid grating structure acting as a resonator with ultrahigh quality factor. This reveals that the physical mechanism responsible for the resonance is quite different from the conventional guided mode resonance (GMR). The hybrid grating consists of a subwavelength grating layer and an un-patterned high-refractive-index cap layer, being surrounded by low index materials. Since the cap layer may include a gain region, an ultracompact laser can be realized based on the hybrid grating resonator, featuring many advantages over high-contrast-grating resonator lasers. The effect of fabrication errors and finite size of the structure is investigated to understand the feasibility of fabricating the proposed resonator.

OCIS codes: (050.2770) Gratings; (140.7090) Ultrafast lasers; (230.5750) Resonators; (050.6624) Subwavelength structures.

References and links

1. C. F. R. Mateus, M. C. Y. Huang, L. Chen, C. J. Chang-Hasnain, and Y. Suzuki, "Broad-band mirror (1.12-1.62 μm) using a subwavelength grating," IEEE Photon. Technol. Lett. **16**(7), 1676–1678 (2004).
2. H. T. Hattori, X. Letartre, C. Seassal, P. Rojo-Romeo, J. L. Leclercq, and P. Viktorovitch, "Analysis of hybrid photonic crystal vertical cavity surface emitting lasers," Opt. Express **11**(5), 1799–1808 (2003).
3. M. C. Y. Huang, Y. Zhou, and C. J. Chang-Hasnain, "Nano electro-mechanical optoelectronic tunable VCSEL," Opt. Express **15**(3), 1222–1227 (2007).
4. C. Sciancalepore, B. B. Bakir, X. Letartre, J. Harduin, N. Olivier, C. Seassal, J. Fedeli, and P. Viktorovitch, "CMOS-compatible ultra-compact 1.55μm emitting VCSELs using double photonic crystal mirrors," IEEE Photonics Technol. Lett. **24**(6), 455–457 (2012).
5. I.-S. Chung, J. Mørk, P. Gilet, and A. Chelnokov, "Subwavelength grating-mirror VCSEL with a thin oxide gap," IEEE Photonics Technol. Lett. **20**(2), 105–107 (2008).
6. I.-S. Chung, V. Iakovlev, A. Sirbu, A. Mereuta, A. Caliman, E. Kapon, and J. Mørk, "Broadband MEMS-tunable high-index-contrast subwavelength grating long-wavelength VCSEL," IEEE J. Quantum Electron. **46**(9), 1245–1253 (2010).
7. I.-S. Chung and J. Mørk, "Silicon-photonics light source realized by III-V/Si-grating-mirror laser," Appl. Phys. Lett. **97**(15), 151113 (2010).
8. G. C. Park, W. Xue, A. Taghizadeh, E. Semenova, K. Yvind, J. Mrk, and I.-S. Chung, "Hybrid vertical-cavity laser with lateral emission into a silicon waveguide," Laser Photonics Rev., doi: 10.1002/lpor.201400418.
9. M. C. Y. Huang, Y. Zhou, and C. J. Chang-Hasnain, "A surface-emitting laser incorporating a high-index-contrast subwavelength grating," Nat. Photonics **1**(2), 119–122 (2007).
10. Y. Zhou, M. Moewe, J. Kern, M. C. Y. Huang, and C. J. Chang-Hasnain, "Surface-normal emission of a high-Q resonator using a subwavelength high-contrast grating," Opt. Express **16**(22), 17282–17287 (2008).
11. T.-T. Wu, S.-H. We, T.-C. Lu, and S.-C. Wang, "GaN-based high contrast grating surface-emitting lasers," Appl. Phys. Lett. **102**, 081111 (2013).

#234571 - $15.00 USD Received 12 Feb 2015; revised 24 Apr 2015; accepted 20 May 2015; published 29 May 2015

12. W. Yang and C. J. Chang-Hasnain, "Physics of high contrast gratings: a band diagram insight," Proc. SPIE **8633**, 863303 (2013).
13. A. Taghizadeh, J. Mørk, and I.-S. Chung, "Hybrid grating reflector with high reflectivity and broad bandwidth," Opt. Express **22**(18), 21175–21184 (2014).
14. R. Magnusson, "Wideband reflectors with zero-contrast gratings," Opt. Lett. **39**(15), 4337–4340 (2014).
15. S. S. Wang and R. Magnusson, "Theory and applications of guided-mode resonance filters," Appl. Opt. **32**(14), 2606–2613 (1993).
16. M. G. Moharam, D. A. Pommet, E. B. Grann, and T. K. Gaylord, "Stable implementation of the rigorous coupled-wave analysis for surface-relief gratings: enhanced transmittance matrix approach," J. Opt. Soc. Am. A **12**(5), 1077–1086 (1995).
17. T. Tamir and S. Zhang, "Modal transmission-line theory of multilayered grating structures," J. of Lightwave Technol. **14**(5), 914–927 (1996).
18. L. Li, "Formulation and comparison of two recursive matrix algorithms for modeling layered diffraction gratings," J. Opt. Soc. Am. A **13**(5), 1024–1035 (1996).
19. P. Lalanne and G. M. Morris, "Highly improved convergence of the coupled-wave method for TM polarization," J. Opt. Soc. Am. A **13**(4), 779–784 (1996).
20. G. Granet and B. Guizal, "Efficient implementation of the coupled-wave method for metallic lamellar gratings in TM polarization," J. Opt. Soc. Am. A **13**(5), 1019–1023 (1996).
21. L. Li, "New formulation of the Fourier modal method for crossed surface relief gratings," J. Opt. Soc. Am. A **14**(10), 2758–2767 (1997).
22. E. Silberstein, P. Lalanne, J. P. Hugonin, and Q. Cao, "Use of grating theories in integrated optics," J. Opt. Soc. Am. A **18**(11), 2865–2875 (2001).
23. J. P. Hugonin and P. Lalanne, "Perfectly matched layers as nonlinear coordinate transforms: a generalized formalization," J. Opt. Soc. Am. A **22**(9), 1844–1849 (2005).
24. V. Karagodsky and C. J. Chang-Hasnain, "Physics of near-wavelength high contrast gratings," Opt. Express **20**(10), 10888–10895 (2012).
25. B. Vial, F. Zolla, A. Nicolet, and M. Commandré, "Quasimodal expansion of electromagnetic fields in open two-dimensional structures," Phys. Rev. A **89**, 023829 (2014).
26. A. Taghizadeh, J. Mørk, and I.-S. Chung. "Comparison of Different Numerical Methods for Quality Factor Calculation of Nano and Micro Photonic Cavities," in Electromagnetic Materials in Microwaves and Optics (METAMATERIALS), 8th International Congress on Advanced (IEEE, 2014), pp. 277–279.
27. N. Gregersen, S. Reitzenstein, C. Kistner, M. Strauss, C. Schneider, S. Hofling, L. Worschech, A. Forchel, T. R. Nielsen, J. Mørk, and J.-M. Gerard, "Numerical and Experimental Study of the Q Factor of High-Q Micropillar Cavities," IEEE J. Quantum Electron. **46**(10), 1470–1483 (2010).
28. M. Shokooh-Saremi and R. Magnusson, "Particle swarm optimization and its application to the design of diffraction grating filters," Opt. Lett. **32**(8), 894–896 (2007).
29. K. X. Wang, Z. Yu, S. Sandhu, and S. Fan, "Fundamental bounds on decay rates in asymmetric single-mode optical resonators," Opt. Lett. **38**(2), 100–102 (2013).
30. V. Karagodsky, C. Chase, and C. J. Chang-Hasnain, "Matrix Fabry-Perot resonance mechanism in high-contrast gratings," Opt. Lett. **36**(9), 1704–1706 (2011).
31. E. Istrate and E. H. Sargent, "Photonic crystal heterostructures and interfaces," Rev. Mod. Phys. **78**(2), 455–481 (2006).
32. C. Peng, Y. Liang, K. Sakai, S. Iwahashi, and S. Noda, "Coupled-wave analysis for photonic-crystal surface-emitting lasers on air-holes with arbitrary sidewalls," Opt. Express **19**(24), 24672–24686 (2011).

1. Introduction

A high contrast grating (HCG) structure is a near-subwavelength grating made of a high-refractive-index material and surrounded by low-refractive-index materials [1]. HCGs can provide extraordinary properties that have not been reported for conventional diffractive gratings with similar periodicity, including high reflectivity $> 99\%$ over a broad bandwidth or high quality (Q) factor resonances ($Q > 10^7$). The broadband nature of the HCG has brought many novel features to vertical-cavity surface-emitting lasers (VCSELs) [2–9]. Also, HCG-resonator lasers with surface normal emission have been demonstrated, with properties of interest for sensing, communication, or display applications [10, 11]. Extensive theoretical studies of HCGs have revealed that the high index-contrast between the grating and surrounding materials is essential for achieving the extraordinary properties [12]. Thus, all HCG designs reported so far employ low refractive index materials such as air and oxides, for the incident as well as exit medium [1–11].

#234571 - $15.00 USD Received 12 Feb 2015; revised 24 Apr 2015; accepted 20 May 2015; published 29 May 2015

Recently, we have found that the combination of a near-subwavelength grating and a cap layer, both made of high-refractive-index materials and surrounded by low-refractive-index materials, as shown in Fig. 1(a), can achieve a high reflectivity over a broader wavelength range than the HCG [13]. Magnusson has independently reported similar result [14]. We refer to this new reflector as a hybrid grating (HG) since it may comprise two different materials, e.g., Si for the grating and InP for the cap layer. At a first look, the HG may appear not to follow the design rules that are known for HCGs [1], since the high-refractive-index cap layer is located next to the grating layer. However, we have found that as long as the entire HG is surrounded by low refractive index materials, the cap layer introduces merely an additional propagation phase delay in the reflection process [13]. Thus, the physical mechanisms providing broadband reflectivity in HCGs and HGs are the same. However, in contrast to the HCG, the HG structure allows the incorporation of a gain material in the cap layer as part of a mirror. This enables the realization of a very short-cavity VCSEL structure consisting of an HG with a gain material, acting simultaneously as a laser mirror and gain element, a very thin cavity layer made of air or oxide, and a second mirror.

In this paper, we show that an HG-based resonator performs just as well as a resonator based on an HCG structure [10]. The mechanism responsible for achieving the high Q-factor resonance is explained, considering interactions between modes in the grating layer, the cap layer, and the input and output media. The structure investigated in this paper bears resemblance to so-called guided-mode resonance (GMR) filters [15]. We explain the similarities and differences, highlighting that HG resonators may achieve Q-factors that are several orders of magnitude higher than conventional GMR filters. Then, the effect of fabrication errors and finite extent of the grating on the resonator properties are investigated and discussed. This discussion focuses the potential of the HG resonator structure as a diode laser with a moderate Q factor.

The HG resonator-based laser (hereafter called HCG resonator laser) structure could have several advantages compared to the HCG resonator laser structure [10]. In the HCG resonator laser structure, a gain material is integrated inside the grating bars while the HG resonator laser structure has a gain material in the cap layer. In the cap layer, metal contacts can be formed for electrical pumping in a similar way as in intracavity-contacted VCSELs. When the current is injected into the gain material, the HG resonator laser structure can have a considerably smaller series resistance as well as a much smaller surface recombination. Furthermore, the HG resonator laser structure can have better heat dissipation capability. The heat generated inside the gain material can be spread out laterally in the InP cap layer as well as vertically into the Si grating layer while in the HCG resonator laser structure heat can be dissipated only laterally along the grating bars since the structure is surrounded by air. Therefore, the HG resonator laser structure appears promising in many applications where compact high-speed laser is required.

2. Device structure and simulation method

Figure 1(a) shows a schematic view of the investigated HG structure. It is assumed that a grating is formed in the silicon layer of a silicon-on-insulator (SOI) wafer and a cap layer made of InP is directly wafer-bonded to the grating layer. Thus, the input and output media are air and SiO_2, respectively. The HG parameters that are varied in the design are the grating layer thickness, t_g, the grating period, Λ, the grating bar filling ratio (duty cycle), f, and the cap layer thickness, t_c. Our first goal is to identify an HG structure with a high Q-factor at a wavelength of 1550 nm by varying these parameters.

The numerical results presented in the paper are obtained, based on an in-house developed simulator, which employs rigorous coupled wave analysis (RCWA) method [16, 17] in combination with the scattering matrices [18]. The RCWA method is also called as Fourier modal method (FMM). We used a two-dimensional (2D) version of the simulator to study the high-Q

#234571 - $15.00 USD Received 12 Feb 2015; revised 24 Apr 2015; accepted 20 May 2015; published 29 May 2015

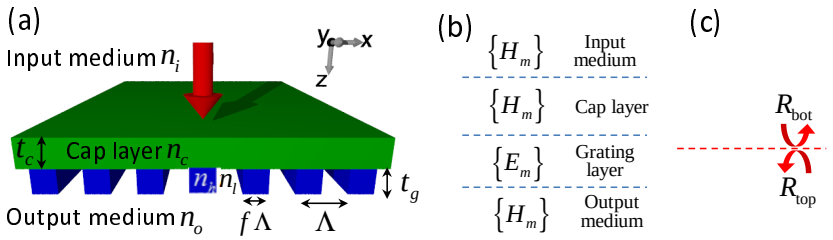

Fig. 1. (a) Schematic view of the investigated HG structure with parameter definitions. Refractive indices: n_h=3.48, n_l=1, n_i=1, n_o=1.47, and n_c=3.166. (b) Bloch modes in each layer. (c) Reflectivity matrices defined at a specific plane within the structure.

resonance mechanism of HG structures (Section 3) as well as the fabrication tolerance (Section 4). An efficient algorithm with fast convergence for TM polarization was employed [19, 20]. Convergence of Q-factor value could be achieved with 151 harmonics. In 2D simulations, the grating is assumed to be infinitely periodic in the x direction and infinitely long in the y direction. A three-dimensional (3D) implementation of the of FMM [21] with absorbing boundary conditions implemented as a nonlinear coordinate transformation [22, 23], was used to investigate the finite size effect on the Q-factor (Section 4). In the 3D version, the absorbing boundary is used to reduce the interaction between adjacent super cells due to the artificial periodicity, which is an inherent properties of FMM. In the RCWA formalism, each layer has its own set of Bloch modes, as shown in Fig. 1(b). The grating layer, featuring a subwavelength period, typically has one to three Bloch modes with a real propagation constant, β_m in the z direction [24]. In homogeneous layers, e.g. the cap layer, each Bloch mode corresponds to a single spatial harmonic (or diffraction order) [16].

For Q-factor estimation, a method based on the quasi-normal mode (QNM) [25] picture is employed among several approaches [26], due to its accuracy and numerical efficiency for both 2D and 3D simulations. In this picture, a resonator is viewed as a passive open system with only out-going emission from the resonator, which determines the boundary conditions. Its resonating modes are referred to as quasi modes [25], since they decay with time. The field evolution during one round trip in the cavity is expressed by a matrix $U = R_{\text{bot}}R_{\text{top}}$ where R_{top} and R_{bot} are the reflectivity matrices from the top and the bottom sections of the structure, respectively, as shown in Fig. 1(c). They are expressed in terms of the Bloch mode sets. Similar to a Fabry Perót resonator, a resonance occurs when an eigenvalue R_r of the matrix U becomes close to one. Then, the Q-factor of the mode is given by [27]

$$Q = \frac{-\lambda_r}{2(1-R_r)}\frac{\partial}{\partial\lambda}\arg(R_r). \tag{1}$$

where λ_r is the wavelength at which the phase of R_r is zero.

For the reflectivity calculations, it is assumed that light is vertically incident from the input medium to the cap layer. In all simulations, transverse magnetic (TM) polarized light, i.e., electric field perpendicular to the grating bars is considered. Similar results can be obtained for transverse electric (TE) polarized light by changing the design parameters.

3. High-Q resonances in a hybrid grating structure

Firstly, a coarse reflectivity scanning over wavelength and HG parameters, i.e., Λ, f, t_c, and t_g is performed. To reduce the number of parameters without loss of generality, all the length scales are normalized with respect to Λ. The reflectivity contour maps of a HG as a function of λ/Λ

#234571 - $15.00 USD Received 12 Feb 2015; revised 24 Apr 2015; accepted 20 May 2015; published 29 May 2015

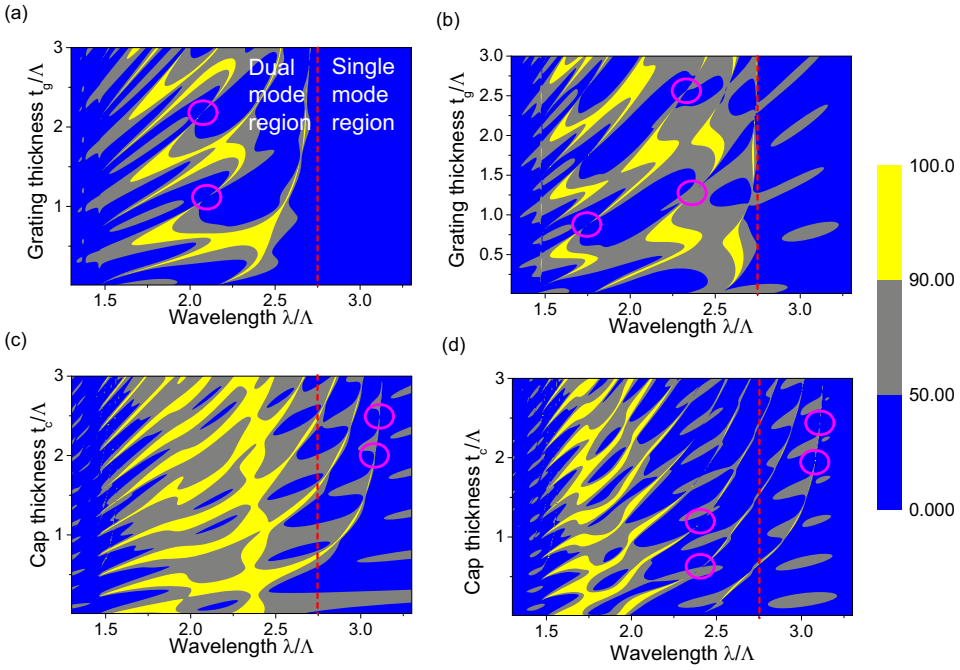

Fig. 2. Contour maps of the reflectivity (color scale) versus normalized wavelength and grating thickness (a,b) or normalized wavelength and cap thickness (c,d) at f=50% for TM polarized light. (a) t_c/Λ=0.4, (b) t_c/Λ=0.6, (c) t_g/Λ=0.6, (d) t_g/Λ=1.35.

and t_g/Λ are plotted in Figs. 2(a) and 2(b) for two different cap layer thicknesses. Results look similar to the simulation results obtained for HCGs (see e.g. [24]). The checkerboard pattern seen in these contour maps reflects the interference between several grating Bloch modes and is similar to the HCG case [24]. The single and dual mode regimes in Fig. 2(a) denote the wavelength ranges with one and two propagating modes in the grating layer, respectively. As in HCGs, high-Q resonances are found close to anti-crossing points in the dual mode regime, some of the ”candidate” points for high-Q resonances are indicated by magenta circles in Fig. 2.

In order to discuss the influence of the cap layer thickness t_c, two reflectivity contour maps as a function of λ/Λ and t_c/Λ for two values of t_g are plotted in Figs. 2(c) and 2(d). High reflectivity lines extend into the single-mode regime, while they are found only within the dual mode regime in Figs. 2(a) and 2(b). Candidate points for resonances are found in both regimes. Note that the resonances found in different regimes have different origins and properties. The resonances observed in the single mode regime, henceforth referred to as type-I resonances, have the same physical origin as the resonances found in conventional GMR-based filters [15]. This type-I resonance is due to the constructive interference of the diffraction orders +1 and -1 in *the cap layer* with total internal reflection at the (air)-(cap layer) interface. Its characteristic feature is that at normal incidence, the diffraction orders +1 and -1 result in two resonance peaks degenerate at the same wavelength in the reflectivity spectrum, but for a finite angle of incidence the peaks will separate spectrally [15]. This resonance type is also found in conventional shallow etched grating structures. It typically has a low Q-factor because the diffraction orders +1 and -1 inside the cap layer result in the appearance of diffraction order 0 when reflected again

#234571 - $15.00 USD Received 12 Feb 2015; revised 24 Apr 2015; accepted 20 May 2015; published 29 May 2015

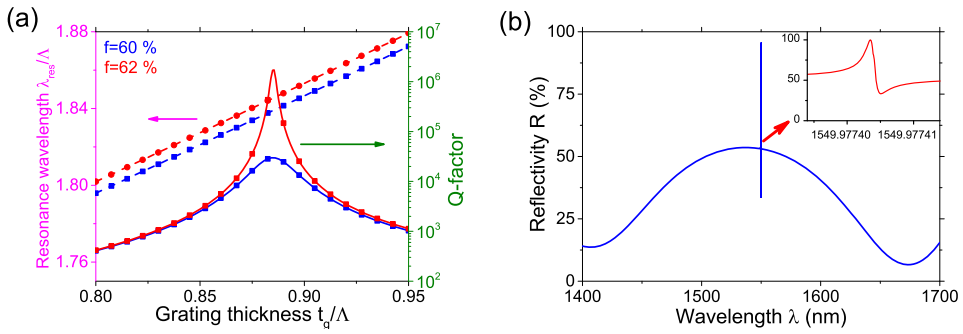

Fig. 3. (a) Resonance wavelength (dashed lines) and Q-factor (solid lines) as a function of grating thickness around a candidate point for resonance at two values of the duty cycle, f=60 % (blue lines) and f=62 % (red lines). The Q-factor depends sensitively on the structure parameters. (b) Reflectivity spectrum for TM-polarized light of an HG structure with ultrahigh Q-factor found by PSO with Λ=853.5 nm, t_g=742.3 nm, f=61.6 %, t_c=830.5 nm.

from the grating and the 0-th order component is lossy at the (air)-(cap layer) interface.

The resonances found only in the dual mode regime, the main focus of this paper, are referred to as type-II resonances, and have a different origin and different properties. As explained below in detail, they originate from the constructive interference of two Bloch modes in *the grating layer*. Since this constructive interference condition requires a certain grating thickness, the type-II resonance is sensitive to the grating thickness while the type-I resonance is not. Type-II resonances may have much higher Q-factor than type-I. Furthermore, a type-II resonance peak in the reflection spectrum at normal incidence does not separate into two peaks but shifts with a small incidence angle. Type-II resonances are not observed in conventional GMR-based grating filters.

As shown in Fig. 3(a), the Q-factor of a type-II resonance is very sensitive to small changes in HG parameters, while its resonance wavelength is relatively insensitive. Thus, after finding several high-Q candidate parameter sets from a coarse scanning of parameters, several runs using particle swarm optimisation (PSO) technique [28] were performed around each candidate set to find the local solution that gives the highest possible Q-factor. Without resorting to the use of PSO, very fine-resolution scan are required due to the sensitiveness of the Q-factor, demanding significant computational efforts.

Using PSO, several designs are identified that result in ultra-high Q-factors. Figure 3(b) shows an example of the reflectivity spectrum for an optimal structure with a Q-factor of 1.12×10^9. This type-II resonance is of the Fano type [29], which means that the resonance occurs as a result of the interference of discrete modes in the HG structure with continuous modes outside the structure. Note that as shown in the inset of Fig. 3(b), this resonance reaches 100% reflectivity but not 100% transmissivity. The reason is that the HG structure inherently does not possess mirror symmetry along the z direction, which results in different decay rates of the electromagnetic energy stored in the HG structure into input and output regions [29]. In contrast, HCG resonators suspended in air have mirror symmetry and the reflectivity varies from 100% to 0% around a resonance peak [10, 30].

Figure 4(a) shows the field profile of this high-Q resonance excited by a TM polarized plane wave incident from the air side. The field is strongly enhanced in the cap layer as well as in the grating layer. To get insight into the field confinement properties of the structure, we have plotted the field strength of different spatial harmonics in Fig. 4(b). As described in the previous

#234571 - $15.00 USD Received 12 Feb 2015; revised 24 Apr 2015; accepted 20 May 2015; published 29 May 2015

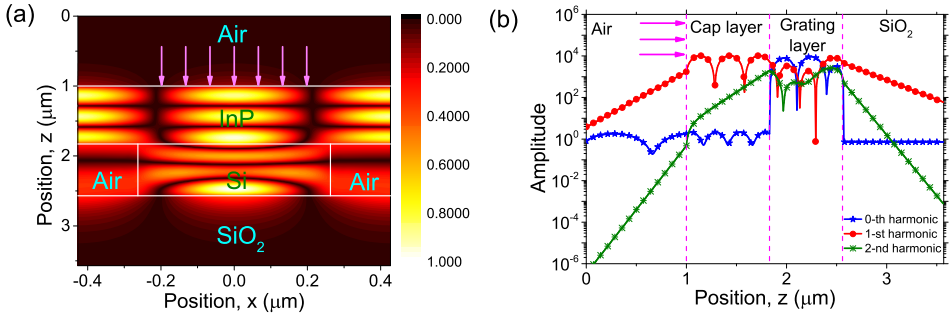

Fig. 4. (a) Normalized magnetic field profile $|H_y|$ for the HG structure of Fig. 1(a), excited by an incident plane wave with the same wavelength as the resonance wavelength found in Fig. 3(b). (b) Amplitudes of the magnetic modal fields in dB scale for 0-th, 1-st and 2-nd spatial harmonic inside all the layers at the resonance wavelength. TM polarized light is incident from the left.

section, these spatial harmonics are the Bloch modes in the cap layer. But for the grating layer, the harmonics contributions from two Bloch modes are added together to plot this figure. It is noteworthy in Fig. 4(b) that the field in the cap layer only contains the 1-st spatial harmonic component, while the grating layer contains the 0-th and 2-nd spatial harmonics as well. This observation is a clue to understanding how such an ultrahigh Q-factor resonance appears in the HG structure.

The signal flow graph (SFG) shown in Fig. 5 illustrates how Bloch modes of the type-II resonance interact with each other at each of the interfaces. The grating layer has two propagating Bloch modes, E_1 and E_2. Both the input (air) and output (SiO_2) media have one propagating harmonic, H_0 while the cap layer has three propagating harmonics, H_0 and $H_{\pm 1}$, due to its high refractive index. The red arrows denote the interactions between modes taking place at interfaces and the green arrows show the mode propagations in each layer. The number besides each dot is the mode coefficient. At the (cap layer)-(grating layer) interface, the excitation of H_0 is very small (c.f. Fig. 4(b)) since the coupling from E_1 and E_2 to H_0, and the self-coupling to H_0 cancel each another at the interface. As a result, the loss at the (air)-(cap layer) interface H_0 is very small. However, the couplings to $H_{\pm 1}$ do not cancel efficiently, resulting in strong excitation of the first harmonic component in the cap layer as observed in Fig. 5. At the (grating layer)-(SiO_2) interface, the 0-th harmonic components of E_1 and E_2 cancel each other, resulting in very small coupling to H_0 in the SiO_2 layer. As shown in the (air)-(cap layer) and (grating layer)-(SiO_2) interfaces, the only loss channel from the HG resonator to the input and output media is through H_0, since other higher-order harmonics become evanescent due to the subwavelength periodicity. Thus, the overall loss becomes very small, which explains the observation of very high Q-factors.

4. Fabrication tolerances and finite size effect

We are interested in applications of HG resonator structure as a laser with a moderate Q-factor and a size of 10 to 15 μm and would estimate the effect of fabrication-related deviations of geometrical parameters from the designed values, on the Q factor. For this estimation, Monte Carlo analysis is employed, assuming that within this length scale of 10 to 15 μm, the fabrication-related deviations of the grating period and bar width are not completely random, rather locally synchronized. In this analysis method, simulations are performed for a large number of param-

#234571 - $15.00 USD Received 12 Feb 2015; revised 24 Apr 2015; accepted 20 May 2015; published 29 May 2015

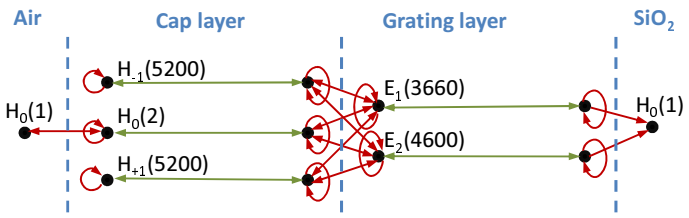

Fig. 5. Signal flow graph for an HG structure at the resonance wavelength of Fig. 3(b). The black dots represent the propagating modes in the different layer; the red arrows show the interactions between modes at each interface; the circular red arrows bring self-couplings; the green arrows illustrate the propagations in each layer. The numbers given besides the dots are the mode coefficients.

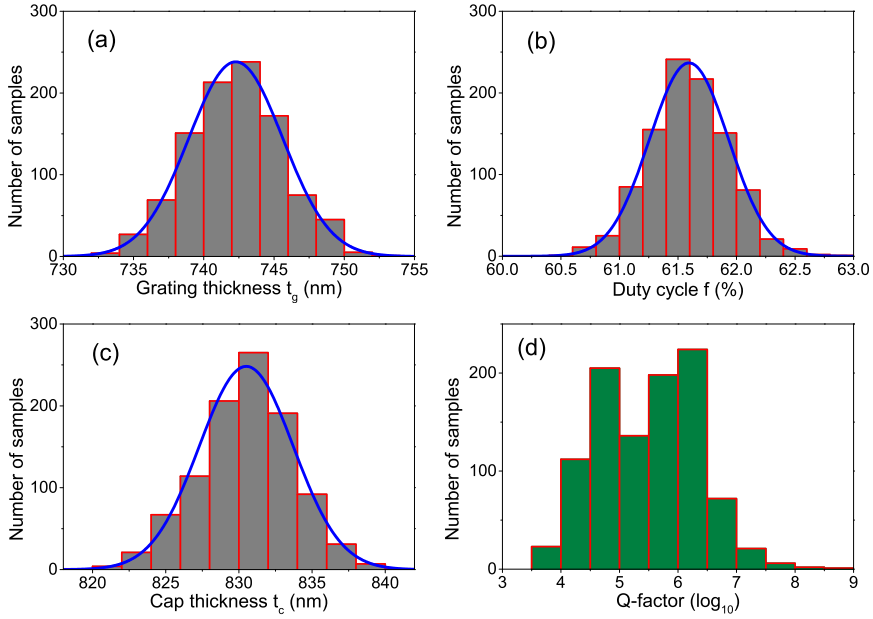

Fig. 6. Monte Carlo analysis of fabrication tolerance. Distributions of (a) grating thickness, (b) duty cycle, (c) cap layer thickness. and (d) resulting Q-factor distribution.

eters, which are chosen from a Gaussian probability distribution and the results are aggregated. As shown in Figs. 6(a)-6(c), variations in grating thickness, duty cycle, and cap layer thickness are analyzed. The variations are assumed to be ± 10 nm for the cap layer and grating layer thickness and $\pm 1\%$ for the duty cycle, i.e., ± 8 nm for the grating bar width. These fabrication errors often occur in epitaxial growth and e-beam lithography with an image transfer to a hard mask followed by dry etching. A total of 1000 simulations is performed, each one being referred to as a sample. The Q-factor distribution in Fig. 6(d) shows that all simulated structures have Q-factors higher than 6000 and 98% of the samples have Q-factors above 10^4, which is sufficiently high for laser applications of our interest.

In a real HG resonator with a finite number of periods and finite length of grating bars, the lateral loss from the end of the grating bars will reduce the Q-factor. This reduction is estimated by performing a 3D simulation. The simulated structure has 21 grating bars in the x direction, is 12 μm long in the y direction and is truncated with air outside. The field profile is

#234571 - $15.00 USD Received 12 Feb 2015; revised 24 Apr 2015; accepted 20 May 2015; published 29 May 2015

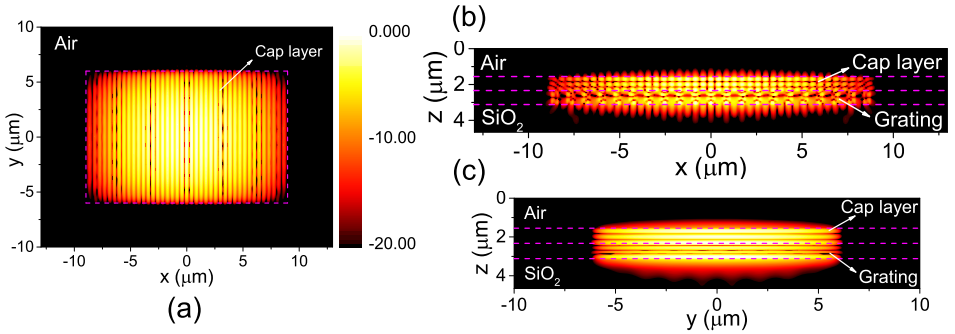

Fig. 7. Normalized mode profiles $|H_y|$ in dB of an HG resonance in (a) *x*-*y* plane in the cap layer, (b) *x*-*z* plane, and (c) *y*-*z* plane.

shown in Fig. 7 and the measured Q-factor is 12000. It is observed in plots with finer details that the scattering loss causing the reduction in Q-factor occurs mostly downwards into SiO_2 layer. The observed Q-factor is acceptable for most laser diode designs. It is also similar to the value obtained for HCG-based resonators [10]. This Q-factor can be considerably increased by simply increasing the size of the structure or introducing heterostructures in the grating in both *x* and *y* directions. The heterostructures that are used in photonic crystal structures [31] can be introduced in a straightforward manner by changing the grating duty cycle or period at the boundaries [4]. Also, we expect that similar to photonic crystal surface-emitting lasers [32], it should be possible to design the resonator with enhanced radiation power in specific direction.

5. Conclusion

We have shown that a hybrid grating (HG) structure can work as an ultrahigh Q-factor resonator and analysed the origin of the high-Q resonances. We have found that the cancellation of the DC component of two propagating modes of the grating layer at the interfaces to surrounding layers leads to high-Q resonances, which is similar to the resonances appearing in high contrast grating (HCG) resonators. Also we have shown that the resonances of an HG structure differ from those of grating filters, highlighting that HG resonators may achieve Q-factors that are several orders of magnitude higher than conventional GMR filters.

Given typical fabrication errors and finite extension of 10 to 15 μm, the Q factor of a HG resonator drops from a ultrahigh value to a moderate value that is still sufficient for laser diode applications. Therefore, the HG resonator based laser structure with a gain material in the cap layer appears promising, featuring a smaller series resistance, less surface recombination loss, and a better heat dissipation capability than the HCG resonator-based laser structures.

Acknowledgments

The authors gratefully acknowledge support by the Danish Council for Independent Research through FTP project (Grant No. 0602-01885B) as well as Villum Fonden via the VKR Center of Excellence NATEC.

#234571 - $15.00 USD Received 12 Feb 2015; revised 24 Apr 2015; accepted 20 May 2015; published 29 May 2015